PAPER

Space charge limited conduction mechanism in GaAsSb nanowires and the effect of *in situ* annealing in ultra-high vacuum

IOP Publishing Nanotechnology
Nanotechnology 31 (2020) 025205 (8pp) https://doi.org/10.1088/1361-6528/ab47aa

Space charge limited conduction mechanism in GaAsSb nanowires and the effect of *in situ* annealing in ultra-high vacuum

Mehul Parakh[1], Sean Johnson[2], Rabin Pokharel[1], Priyanka Ramaswamy[2], Surya Nalamati[2], Jia Li[1] and Shanthi Iyer[1,2]

[1] Nanoengineering, Joint School of Nanoscience and Nanoengineering, North Carolina A&T State University, Greensboro, NC 27401, United States of America
[2] Department of Electrical and Computer Engineering, North Carolina A&T State University, Greensboro, NC 27411, United States of America

E-mail: iyer@ncat.edu

Received 4 June 2019, revised 29 August 2019
Accepted for publication 25 September 2019
Published 14 October 2019

Abstract

In this work, the first observation of the space charge limited conduction mechanism (SCLC) in GaAsSb nanowires (NWs) grown by Ga-assisted molecular beam epitaxial technique, and the effect of ultra-high vacuum *in situ* annealing have been investigated. The low onset voltage of the SCLC in the NW configuration has been advantageously exploited to extract trap density and trap distribution in the bandgap of this material system, using simple temperature dependent current–voltage measurements in both the ensemble and single nanowires. *In situ* annealing in ultra-high vacuum revealed significant reduction in the trap density from $10^{16}\,cm^{-3}$ in as-grown NWs to a low level of $7 \times 10^{14}\,cm^{-3}$ and confining wider trap distribution to a single trap depth at 0.12 eV. A comparison of current conduction mechanism in the respective single nanowires using conductive atomic force microscopy (C-AFM) further confirms the SCLC mechanism identified in GaAsSb ensemble device to be intrinsic. Higher current observed in current mapping by C-AFM, increased 4 K photoluminescence (PL) intensity along with reduced full-width half maxima and more symmetric PL spectra, and reduced asymmetrical broadening with increased TO/LO mode in room temperature Raman spectra for *in situ* annealed NWs again attest to effective annihilation of traps leading to the improved optical quality of NWs compared to as-grown NWs. Hence, the *I–V–T* analysis of the SCLC mechanism has been demonstrated as a simple approach to obtain information on growth induced traps in the NWs.

Keywords: GaAsSb, III–V material, conductive atomic force microscopy (C-AFM), space charge limited current (SCLC), temperature dependent current–voltage (*I–V–T*), Nanowire (NW), annealing

(Some figures may appear in colour only in the online journal)

Introduction

Semiconductor nanowires have generated great interest due to their one-dimensional architecture with high surface to volume ratio enabling enhanced light absorption, elastic relaxation of the lattice mismatch-induced strain at edges, sub-wavelength optical phenomenon, and quantum size effects [1, 2]. Further, the flexibility of integrating different material systems in NW configuration and a wider choice of substrates that is not conceivable in thin films broadens the scope of potential opportunities by using this as a building block for fabricating wide range of high-performance NW

optoelectronic devices at a lower cost as in photovoltaic devices [3], UV nanolasers [4] and FETs [5]. Among the III–V material system, GaAsSb bandgap energy covers the important telecommunication wavelength in the electromagnetic spectrum for near-infrared telecommunication, computing, and optical interconnects [6].

It is well known that in ternary III–V NW material alloy systems, inhomogeneous composition and phase separation [7], atomic ordering [8], and miscibility gap [9] phenomena can have deleterious effects on electrical and optical properties for NW devices operating at room temperature (RT). In the GaAsSb material system, in particular in the NW configuration, the electronic and the optoelectronic properties are strongly dependent on Sb concentration due to its inhomogeneous distribution in NWs both axially and radially [10], and also on the presence of point defects such as intrinsic Ga_{Sb} antisite defects and Ga vacancies [11, 12].

Further, the NW configuration provides an additional source of defects compared to their thin film counterparts due to the presence of planar defects namely, stacking faults or twins during NW growth [13] particularly when grown in core–shell configuration. The foreign catalyst used in the NW growth may act as a deep trap [14] or as a shallow donor in NWs [15], while the surface roughness and step edges on the NW surface [16] can contribute as a source of electrical defect and degrade the performance of the NW device.

The one-dimensional architecture of NWs commonly leads to the presence of more than one conduction mechanism in the NWs [17, 18]. The dominance of a specific mechanism for a given growth technique depends on numerous parameters, namely the composition of the NW, the physical dimension, the bias range, the NW architecture, and so forth. One of the common conduction mechanisms that have been observed in different types of NWs is the space charge limited current (SCLC) [18–22]. This arises when the injected charge carriers dominate over the thermally generated carriers [23] and are generally the case in intrinsic NWs. The one-dimensional geometry, along with the small footprint of the NWs enables the onset of the SCLC mechanism to occur at a much lower voltage than in the bulk material. The analysis of SCLC mechanism therefore offers a pathway to gain more insight in the nature and density of the traps present in NWs.

Hence, in this work, we have investigated the *I–V* characteristics of GaAsSb NWs grown by Ga-assisted molecular beam epitaxy (MBE), with emphasis on the region exhibiting the SCLC mechanism. Ga-assisted growth eliminated the effect of foreign catalyst. Room temperature *I–V* characterization has been carried out on single and ensemble NWs. The temperature dependent *I–V* characteristics on ensemble NW devices have been used to extract the trap level and trap density distribution throughout the NW. We show that ultra-high vacuum *in situ* annealing of the NWs is an effective tool in lowering the trap density as well as its distribution in the NW leading to enhanced PL intensity and suppressed LO mode in the Raman spectra. This is also consistent with the observed improvement in the device performance after *in situ* annealing of GaAsSb P–I NW ensemble devices reported by Sharma *et al* [24]. Therefore, simple current–voltage (*I–V*) measurements and its temperature dependence can be used as a powerful diagnostic tool for quantitative analysis of the electrical transport parameters and defect-related behavior of the NW, as extracting the values of the transport parameters by conventional Hall measurements commonly used in thin films or bulk materials is more tedious due to the nanoscale nature of the contact formation on NWs.

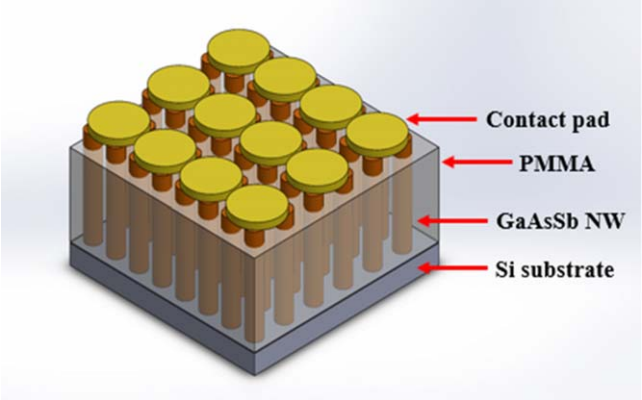

Figure 1. Schematic of the GaAsSb ensemble NW device.

Experimental details

The GaAsSb NWs used in this work are synthesized via a self-catalyzed VLS growth approach using solid source EPI 930 MBE system on Si (111) substrates. GaAsSb core and GaAlAs shell were grown at 590 °C and 465 °C, respectively. For this study, two sets of samples were grown. One was as-grown and the other with *in situ* annealing in ultra-high vacuum at 465 °C for 10 min before the growth of the GaAlAs shell. More details of the growth are provided elsewhere [24, 25]. The surface morphology of the NWs was examined using a Carl Zeiss Auriga-BU field emission scanning electron microscope (FESEM) at an operating voltage of 5 KV.

For the electrical characterization, the NW ensemble was spin-coated with polymethyl methacrylate (PMMA) layer, and the NW tips were exposed by chemical etching. Circular contact pads of Au/Ti (150/20 nm) and Au/Ni (150/20 nm) were made as top and bottom contacts, respectively, using electron beam deposition for the two-probe *I–V* measurement. The device schematic is displayed in figure 1.

Temperature-dependent current–voltage (*I–V–T*) curves of the NW ensembles were obtained using a Keithley 4200 semiconductor parameter analyzer system used in conjunction with a Lake Shore TTPX probe station equipped with radiation shield in an N_2 purged environment for two-probe measurements.

Also, conductive atomic force microscopy (CAFM Asylum MFP-3D Origin) operating in contact mode was used for single NW for RT *I–V* characteristics. A Pt coated Si cantilever of radius ~20 nm and a spring constant of 18 N m^{-1} was used. *I–V* measurements were carried out by positioning AFM probe on the NW tip and providing

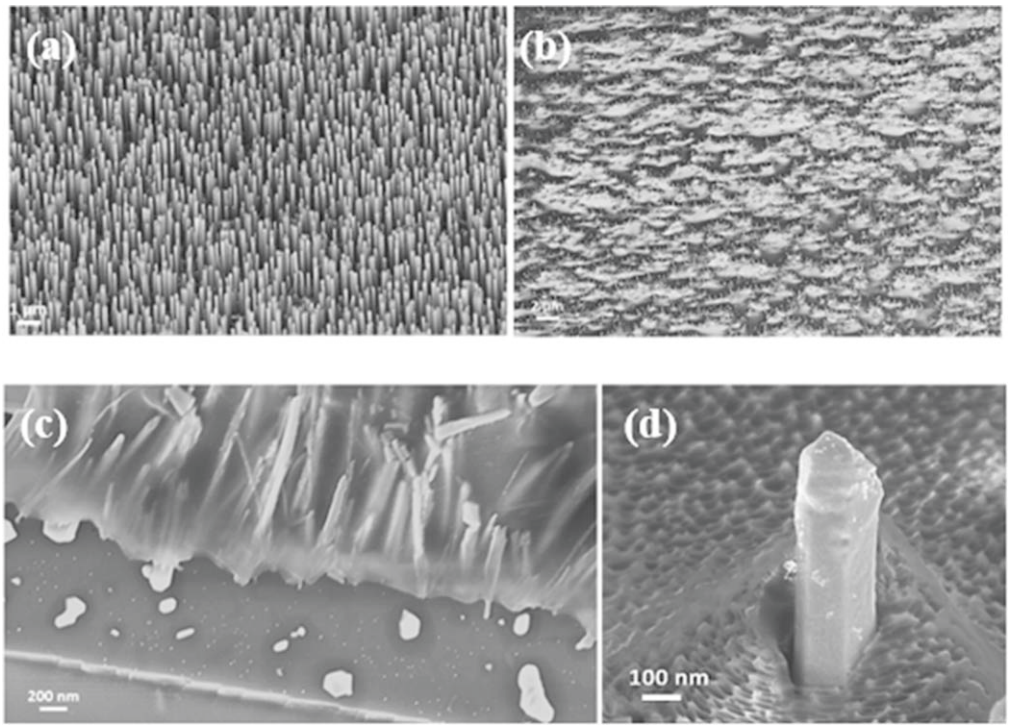

Figure 2. FESEM images: (a) GaAsSb NWs on Si (111) substrate, (b) top view of GaAsSb NW ensemble spin-coated with PMMA, (c) tilted view of NW ensemble embedded in PMMA at the edge of the substrate and (d) an NW tip exposed above PMMA.

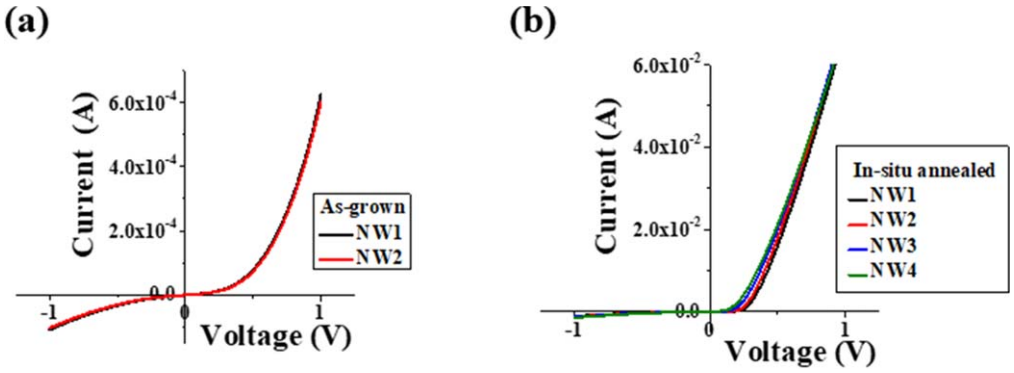

Figure 3. *I–V* characteristics of different NW ensemble: (a) as-grown and (b) *in situ* annealed.

secondary contact on the top side of the substrate with voltage bias varying from −1 to 1 V [26].

Micro-photoluminescence (μ-PL) system was also used for the assessment of the optical properties of as-grown and *in situ* annealed NWs, which employs 633 nm He–Ne laser as the source of excitation, 0.32 m double grating monochromator for the wavelength dispersion and InGaAs detector with conventional lock-in techniques. A closed cycle optical cryostat from the Montana cryostation with the sample chamber interfaced with a fiber-coupled confocal microscope was used to study the variation of PL spectra of the sample between RT and 4 K.

Finally, the vibrational characteristics of the NWs were determined by Raman spectroscopy at RT, which used a He–Ne laser with 633 nm as the excitation source.

Results and discussions

Vertically aligned GaAsSb ensemble NWs of an average length of ∼2.5 μm with a diameter of ∼125 nm were grown on Si (111) substrate. Figures 2(a)–(d) show the FESEM images of these NWs, with top, tilted view and a single NW embedded in PMMA, respectively.

The RT *I–V* characteristics of as-grown and *in situ* annealed ensemble GaAsSb NWs are shown in figures 3(a) and (b), respectively. The *in situ* annealed NW ensembles exhibit two orders of magnitude higher current in the forward bias compared to the as-grown NW ensemble.

However, both the *I–V* curves under forward bias follow a power-law relationship $I \propto V^m$, with $m = 3.8$ for the device before annealing (figure 4(a)), and $m = 2.38$ after annealing

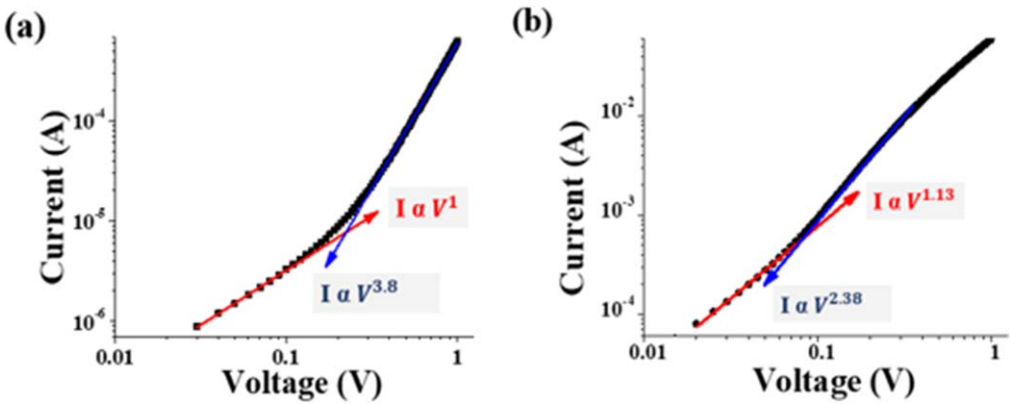

Figure 4. (a) Log–log *I–V* plot for the as-grown, and (b) annealed NW ensemble devices at RT exhibiting linear and power dependence.

(figure 4(b)). In the low bias region, the *I–V* characteristics are almost linear in both types of NWs.

The presence of two slopes in the log–log *I–V* characteristics is indicative of the presence of two different conduction mechanisms, each one dominating over different bias range [18]. The linear *I–V* dependence at lower voltage bias range suggests the dominance of background-free carriers over the injected carriers. At higher bias range, the power-law dependence of the observed *I–V* signature of the SCLC conduction mechanism is attributed to the dominance of injected carriers over the free carriers. The value of the exponent is indicative of the absence or the presence of traps, with 2 being representative of trap free SCLC mechanism, while exponents exceeding 2 is representative of a trap-associated SCLC conduction mechanism [27]. The suppression of free charge carriers and the observation of SCLC mechanism in the NWs are often attributed to arise from the high density of surface states associated with one-dimensional geometry, which is responsible for poor electrostatic shielding of injected charge carriers as well as for large depletion widths at contacts that hinder punch-through of the carriers [28]. Similar reports of observation of SCLC mechanism in other NWs include NWs of GaAs [18, 29], GaSb [19], InN [21], Si [20] and ZnO [22].

To gain a deeper insight into the competitive behavior of injected and free carrier density, temperature dependent *I–V* measurements were carried out on *in situ* annealed ensemble NW device in the temperature region from 200 to 400 K, as illustrated in figure 5. At low and intermediate temperatures ranging from 200 to 325 K, the transition from linear behavior to *I–V* power-law dependency with increasing bias is pronounced, which gradually vanishes with an increase in temperature. At 400 K, the *I–V* exhibits only linear characteristic in the entire bias region investigated. This change in behavior with temperature can be explained based on the injected carriers dominating the conduction mechanism at lower temperatures due to a partial freeze of free carriers in the traps, while at higher temperatures de-trapping of these carriers takes place. This behavior also provides further support to our earlier assignment of the conduction mechanism at a higher bias to the SCLC mechanism. It is to be noted that the combination of the SCLC mechanism and the high density

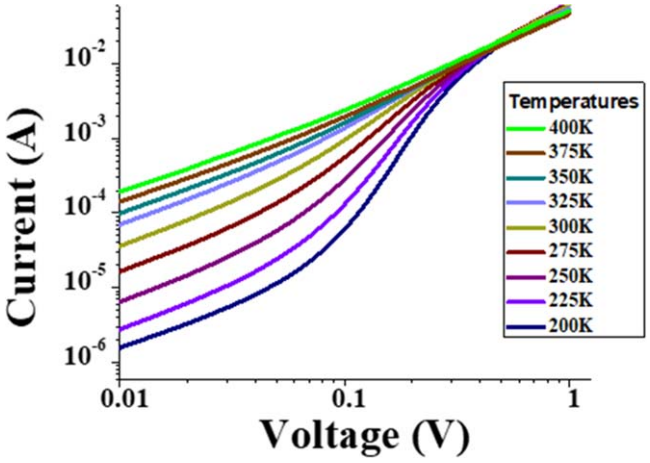

Figure 5. Temperature dependence of *I–V* characteristics of *in situ* annealed NW ensemble device.

of NWs led to the observed high current. Hence, the investigations were limited to a bias voltage of 1 V to prevent any deterioration of the NW characteristics.

These temperature dependent *I–V* characteristics can be used for an estimation of the trap energy level and its density, assuming an exponential trap distribution below the band edge [30]. In such a case, the distribution function for trap density, $N_t(E)$ can be written as:

$$N_t(E) = \frac{H_t}{E_t}\exp\left(\frac{-E}{E_t}\right), \tag{1}$$

where E is the relative energy measured from the bottom of the conduction band, E_t is the characteristic trap energy distribution and is often written in terms of characteristic trap temperature T_c as $E_t = K_b T_c$, K_b being the Boltzmann constant.

This trap distribution gives a power-law dependence of current density on the applied voltage, which is given as [31]:

$$J = q^{1-l}\mu_c N_c\left(\frac{2l+1}{l+1}\right)^{l+1}\left(\frac{l\,\varepsilon_s\varepsilon_0}{l+1\,H_t}\right)^{l}\frac{V^{l+1}}{L^{2l+1}}, \tag{2}$$

where H_t is the density of traps, ε_s is the dielectric constant of the material, ε_0 is the permittivity of free space, μ_c is the carrier mobility, N_c is the density of states in the conduction

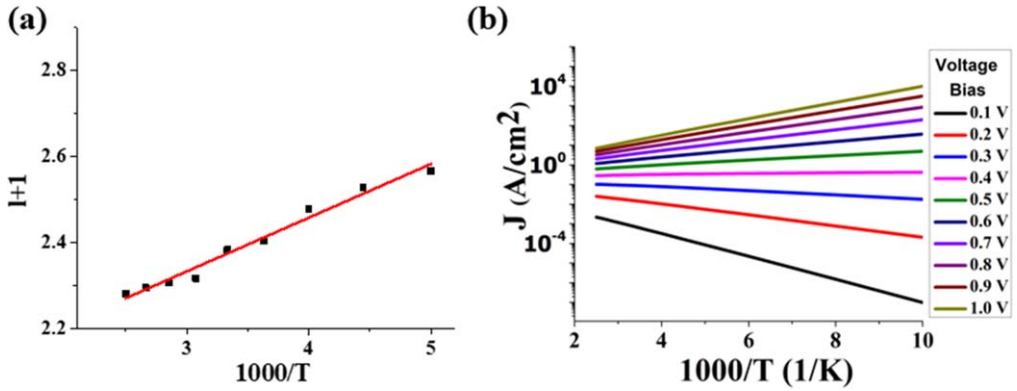

Figure 6. (a) $l + 1$ as a function of inverse temperature, and (b) log J versus $(1/T)$ plot at different voltages, which shows temperature invariance characteristics at $V_c = 0.4$ V.

band, $l = T_c/T$, T is the measurement temperature and 'L' is the NW length.

Using the plot of the variation of parameter $l + 1$ with the inverse of temperature (figure 6 (a)), where $l + 1$ represents the slope of the log J–log V curve in the SCLC regime, the characteristic energy E_t (which is the slope) was computed to be ~0.12 eV. This characteristic trap energy level is in the energy range normally assigned to the defect combination of Ga_{sb} antisite and a complex defect associated with Ga vacancies [12].

The trap density was then determined from the cross-over voltage V_c, which signifies temperature independent current density, using the following equation [30, 31]:

$$V_c = \frac{qH_tL^2}{2\varepsilon_s\varepsilon_0}. \quad (3)$$

The cross-over voltage is determined to be 0.4 V from the extrapolation of log I–log V plot in the SCLC region for different temperatures, where all plots intersect (figure 5). Alternately, V_c can also be viewed as the voltage corresponding to zero activation energy. The invariant nature of temperature dependence of current density at 0.4 V, as illustrated in figure 6(b), further confirms the V_c to be 0.4 V.

The trap density H_t for the NW's was determined to be $\sim 7 \times 10^{14}\,\mathrm{cm}^{-3}$ using simple substitution of values in equation (3). This value of trap density for NW device is lower to those reported in other III–V NW's [19, 29, 32, 33].

Similar I–V measurements were carried out on as-grown GaAsSb NW ensemble. The I–V–T plot of as-grown NWs in figure 7, in contrast to the *in situ* annealed NWs, revealed a distribution of cross-over voltages ranging from 0.2 to 7 V. This is a clear signature of the presence of traps at different energy levels with trap density distribution from $3 \times 10^{14}\,\mathrm{cm}^{-3}$ at 0.2 V to $10^{16}\,\mathrm{cm}^{-3}$ at 7 V in the as-grown NWs.

This suggests that *in situ* annealing in an ultra-high vacuum is effective in the annihilation of the traps leading to a significant reduction in the trap density and its distribution.

Conductive atomic force microscopy (C-AFM) was used for current mapping images, of the ensemble NWs and I–V characteristics on single NW, to reaffirm the results obtained above in the NW ensemble devices. This technique has the advantage to minimize the effect of processing during the ensemble contact fabrication at the NW tip, along with simplicity and rapid turn-around time for characterization. Figures 8(a) and (b) show current mapping images of as-grown and *in situ* annealed NWs by C-AFM. Observation of increased density of circular conductive spots in *in situ* annealed NWs compared to as-grown NWs is clearly indicative of higher number of conducting NWs in the former case. Room temperature log I versus log V plots under forward bias for both these type of SNWs (figures 8(c) and (d)) reveal a linear characteristic at lower bias range and power-law dependence with increasing bias. The exponent of the power-law in as-grown is higher compared to *in situ* annealed NWs. All these data are consistent with the ensemble NW devices, further confirming the presence of the SCLC as the dominant transport mechanism in GaAsSb SNWs with improved conductivity in *in situ* annealed NWs due to the lower trap density. Also, the processing and metallization process for achieving ohmic contacts in the ensemble NWs as well as any contact resistance appear to have negligible effect on the intrinsic SCLC charge transport mechanism in the NWs.

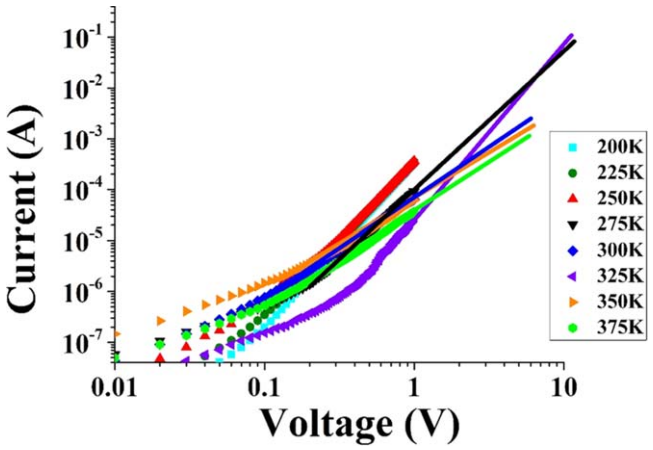

Figure 7. Log I–log V plot for as-grown NW ensemble device.

Next, the effects of *in situ* annealing using the PL characteristics were examined (figure 9). *In situ* annealed GaAsSb NWs show a significant increase in PL intensity and reduced

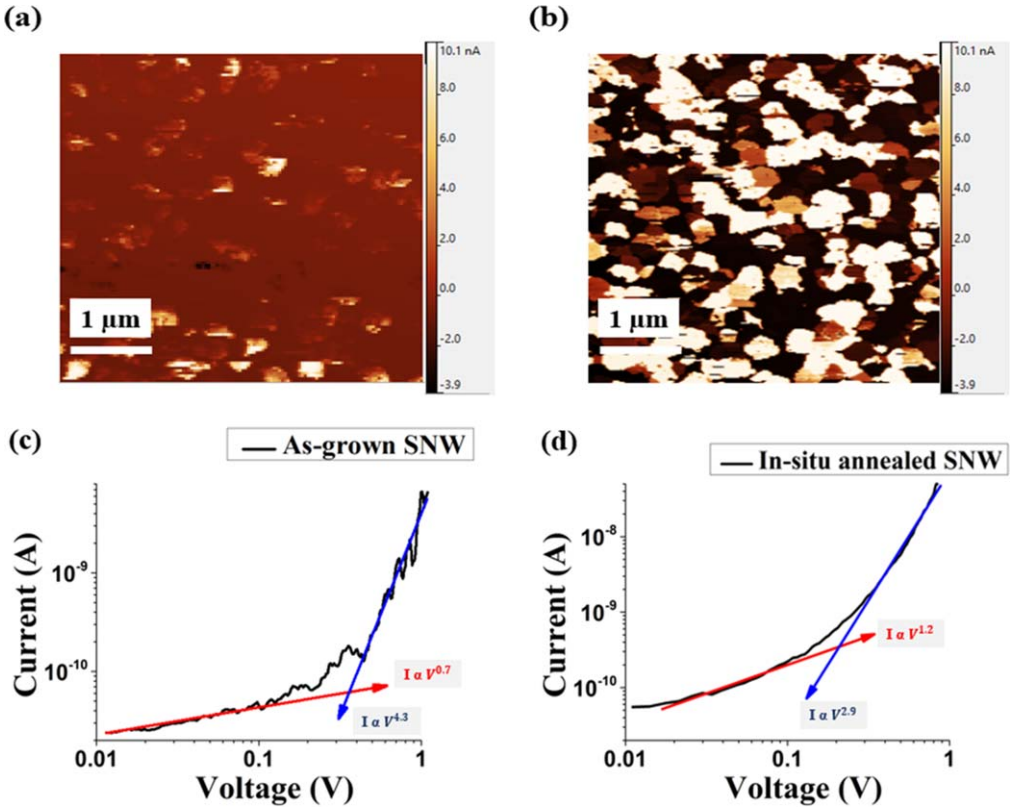

Figure 8. Current mapping images of ensemble NWs using C-AFM: (a) As-grown and (b) *in situ* annealed. Log *I* versus log V plots of SNWs: (c) As-grown and (d) *in situ* annealed.

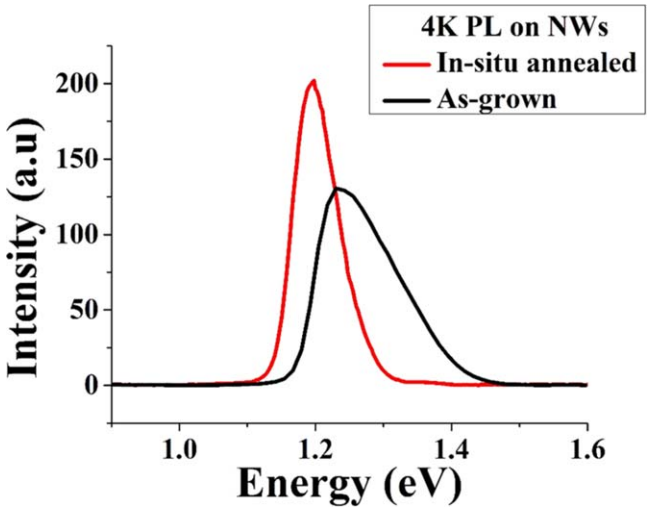

Figure 9. Superimposed PL emission for as-grown intrinsic GaAsSb and *in situ* annealed NWs at 4 K.

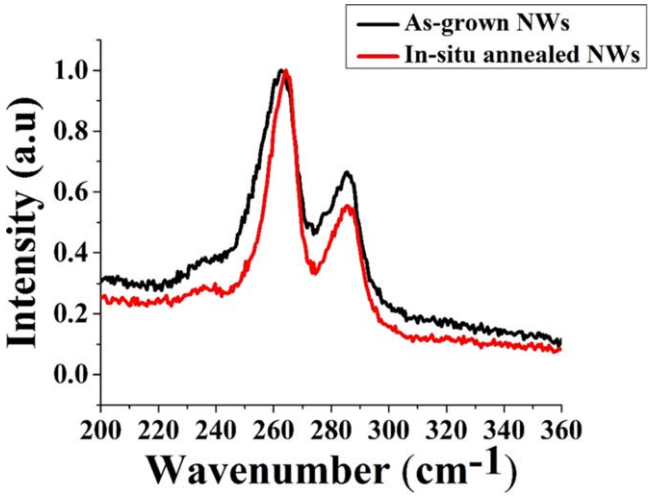

Figure 10. Normalized RT Raman spectra comparison of as-grown and *in situ* annealed GaAsSb NWs.

full-width half maxima (FWHM) compared to as-grown NWs. *In situ* annealing is speculated to provide the thermal energy to annihilate the defects introduced during the growth while also improving the compositional homogeneity, leading to a reduction in the overall density of traps and their distribution in the NWs. Thus, the non-radiative recombination channels are suppressed, yielding enhanced PL intensity in *in situ* annealed NWs compared to as-grown.

Room temperature Raman spectra of as-grown and *in situ* annealed GaAsSb ensemble NWs are compared in figure 10. LO mode intensity is reduced for *in situ* annealed NWs with a concomitant increase in TO/LO ratio compared to as-grown NWs. This difference is attributed to the occurrence of the depletion region at the surface primarily due to the presence of surface state density on the NWs, creating a surface-induced electric field. The suppression of LO intensity suggests the narrowing of the depletion region after *in situ*

annealing, indicative of annihilation of surface trap states [24]. Increased asymmetric broadening in as-grown NWs as compared to *in situ* annealed NWs is indicative of compositional inhomogeneity, and increased disorder in NWs [34]. Thus, *in situ* annealing very likely impacts the trap states both in the core of the NW and at the surface, leading to improved optical and electrical properties of the NWs.

Our findings are consistent with the earlier reports of Sharma *et al* [24] on P–I NW ensemble where a significant improvement in spectral response was observed on devices, which were *in situ* annealed. Thus, the temperature dependence of *I–V* characteristics provides direct evidence of annihilation of the traps on *in situ* annealing and explains the improved optoelectronics properties observed in GaAsSb NWs.

Conclusion

The first observation of the SCLC conduction mechanism in intrinsic GaAsSb SNW (using C-AFM) and ensemble NW device (two-probe measurement) has been discussed. This effect has been exploited to extract trap density and trap level positioning near the band edge using temperature dependent *I–V* measurements. *In situ* annealing in an ultra-high vacuum revealed significant reduction in the trap density from $10^{16}\,\mathrm{cm}^{-3}$ in as-grown NWs to a low level of $7 \times 10^{14}\,\mathrm{cm}^{-3}$ and suppressed wider trap distribution to a single trap depth at 0.12 eV. Increased PL intensity with narrower FWHM in *in situ* annealed NWs and lower LO mode intensity in the corresponding Raman spectra further attest to the annealing-induced annihilation of the traps. Thus, the *I–V–T* measurement in SCLC regime has been successfully shown to identify growth related induced traps.

Acknowledgments

This work is supported by the Air Force Office of Scientific Research (grant #W911NF-19-1-0002) and National Science Foundation (grant #ECCS-1832117). This work was performed at Joint School of Nanoscience and Nanoengineering, a member of the South Eastern Nanotechnology Infrastructure Corridor (SENIC) and National Nanotechnology Coordinated Infrastructure (NNCI), which is supported by the National Science Foundation (ECCS-1542174).

ORCID iDs

Shanthi Iyer https://orcid.org/0000-0002-8163-9943

References

[1] LaPierre R R, Robson M, Azizur-Rahman K M and Kuyanov P 2017 A review of III–V nanowire infrared photodetectors and sensors *J. Phys. D: Appl. Phys.* **50** 123001

[2] Zhang Y, Wu J, Aagesen M and Liu H 2015 III–V nanowires and nanowire optoelectronic devices *J. Phys. D: Appl. Phys.* **48**

[3] Dasgupta N P and Yang P 2013 Semiconductor nanowires for photovoltaic and photoelectrochemical energy conversion *Frontiers Phys.* **9** 289–302

[4] Huang M H, Mao S, Feick H, Yan H, Wu Y, Kind H, Weber E, Russo R and Yang P 2001 Room-temperature ultraviolet nanowire nanolasers *Science* **292** 1897–9

[5] Cui Y, Zhong Z, Wang D, Wang W U and Lieber C M 2003 High performance silicon nanowire field effect transistors *Nano Lett.* **3** 149–52

[6] Deshmukh P, Sharma M, Nalamati S, Reynolds C L, Liu Y and Iyer S 2018 Molecular beam epitaxial growth of high quality Ga-catalyzed $GaAs_{1-x}$ Sb_x ($x > 0.8$) nanowires on Si (111) with photoluminescence emission reaching 1.7 μm *Semicond. Sci. Technol.* **33** 125007

[7] Stringfellow G B 1982 Spinodal decomposition and clustering in III/V alloys *J. Electron. Mater.* **11** 903–18

[8] Ercolani D, Gemmi M, Nasi L, Rossi F, Pea M, Li A, Salviati G, Beltram F and Sorba L 2012 Growth of InAs/InAsSb heterostructured nanowires *Nanotechnology* **23** 115606

[9] Stringfellow G B 1982 Miscibility gaps in quaternary III/V alloys *J. Cryst. Growth* **58** 194–202

[10] Huh J, Yun H, Kim D C, Munshi A M, Dheeraj D L, Kauko H, van Helvoort A T, Lee S, Fimland B O and Weman H 2015 Rectifying single GaAsSb nanowire devices based on self-induced compositional gradients *Nano Lett.* **15** 3709–15

[11] Hakala M, Puska M J and Nieminen R M 2002 Native defects and self-diffusion in GaSb *J. Appl. Phys.* **91** 4988–94

[12] Dyksik M, Motyka M, Kurka M, Ryczko K, Dallner M, Höfling S, Kamp M, Sęk G and Misiewicz J 2016 Photoluminescence quenching mechanisms in type II InAs/GaInSb QWs on InAs substrates *Opt. Quantum Electron.* **48** 401

[13] Davidson F M, Wiacek R and Korgel B A 2005 Supercritical fluid−liquid−solid synthesis of gallium phosphide nanowires *Chem. Mater.* **17** 230–3

[14] Gu G, Burghard M, Kim G T, Düsberg G S, Chiu P W, Krstic V, Roth S and Han W Q 2001 Growth and electrical transport of germanium nanowires *J. Appl. Phys.* **90** 5747–51

[15] Davidson F M, Schricker A D, Wiacek R J and Korgel B A 2004 Supercritical fluid–liquid–solid synthesis of gallium arsenide nanowires seeded by alkanethiol-stabilized gold nanocrystals *Adv. Mater.* **16** 646–9

[16] Ding Y and Wang Z L 2004 Structure analysis of nanowires and nanobelts by transmission electron microscopy *J. Phys. Chem.* B **108** 12280–91

[17] Zhang Z, Yao K, Liu Y, Jin C, Liang X, Chen Q and Peng L M 2007 Quantitative analysis of current–voltage characteristics of semiconducting nanowires: decoupling of contact effects *Adv. Funct. Mater.* **17** 2478–89

[18] Bussone G, Schafer-Eberwein H, Dimakis E, Biermanns A, Carbone D, Tahraoui A, Geelhaar L, Bolivar P H, Schulli T U and Pietsch U 2015 Correlation of electrical and structural properties of single as-grown GaAs nanowires on Si (111) substrates *Nano Lett.* **15** 981–9

[19] Xu W, Chin A, Ye L, Ning C Z and Yu H 2012 Charge transport and trap characterization in individual GaSb nanowires *J. Appl. Phys.* **111** 104515

[20] Alvarez J *et al* 2011 Conductive-probe atomic force microscopy characterization of silicon nanowire *Nanoscale Res. Lett.* **6** 110

[21] Zhao S, Salehzadeh O, Alagha S, Kavanagh K L, Watkins S P and Mi Z 2013 Probing the electrical transport properties of intrinsic InN nanowires *Appl. Phys. Lett.* **102** 073102

[22] Liao Z M, Lv Z K, Zhou Y B, Xu J, Zhang J M and Yu D P 2008 The effect of adsorbates on the space-charge-limited current in single ZnO nanowires *Nanotechnology* **19** 335204
[23] Rose A 1955 Space-charge-limited currents in solids *Phys. Rev.* **97** 1538–44
[24] Sharma M, Ahmad E, Dev D, Li J, Reynolds C L, Liu Y and Iyer S 2019 Improved performance of GaAsSb/AlGaAs nanowire ensemble Schottky barrier based photodetector via *in situ* annealing *Nanotechnology* **30** 034005
[25] Ahmad E, Ojha S K, Kasanaboina P K, Reynolds C L, Liu Y and Iyer S 2017 Bandgap tuning in GaAs1−xSbxaxial nanowires grown by Ga-assisted molecular beam epitaxy *Semicond. Sci. Technol.* **32** 035002
[26] Nalamati S, Sharma M, Deshmukh P, Kronz J, Lavelle R, Snyder D, Reynolds C L, Liu Y and Iyer S 2019 A study of GaAs1-xSbx axial nanowires grown on monolayer graphene by Ga-assisted molecular beam epitaxy for flexible near infrared photodetectors *ACS Appl. Nano Mater.* **2** 4528–37
[27] Zhu Y B and Ang L K 2015 Non-uniform space charge limited current injection into a nano contact solid *Sci. Rep.* **5** 9173
[28] Talin A A, Leonard F, Swartzentruber B S, Wang X and Hersee S D 2008 Unusually strong space-charge-limited current in thin wires *Phys. Rev. Lett.* **101** 076802
[29] Schricker A D, Davidson F M, Wiacek R J and Korgel B A 2006 Space charge limited currents and trap concentrations in GaAs nanowires *Nanotechnology* **17** 2681–8
[30] Kumar V, Jain S C, Kapoor A K, Poortmans J and Mertens R 2003 Trap density in conducting organic semiconductors determined from temperature dependence of $J-V$ characteristics *J. Appl. Phys.* **94** 1283–5
[31] Rafiq M A 2018 Carrier transport mechanisms in semiconductor nanostructures and devices *J. Semicond.* **39** 061002
[32] Simpkins B S, Mastro M A, Eddy C R, Hite J K and Pehrsson P E 2011 Space-charge-limited currents and trap characterization in coaxial AlGaN/GaN nanowires *J. Appl. Phys.* **110** 044303
[33] Rasool K, Rafiq M A, Ahmad M, Imran Z, Batool S S, Nazir A, Durrani Z A K and Hasan M M 2015 Charge injection and trapping in TiO_2 nanoparticles decorated silicon nanowires arrays *Appl. Phys. Lett.* **106** 073101
[34] Ahmad E, Karim M R, Hafiz S B, Reynolds C L, Liu Y and Iyer S 2017 A two-step growth pathway for high Sb incorporation in GaAsSb nanowires in the telecommunication wavelength range *Sci. Rep.* **7** 10111